High Microvascular Endothelial Water Permeability in Mouse Lung Measured by a Pleural Surface Fluorescence Method

Ethan P. Carter, Bence P. Ölveczky, Michael A. Matthay, and A. S. Verkman
Departments of Medicine and Physiology, Cardiovascular Research Institute, University of California, San Francisco, California 94143 USA

ABSTRACT Transport of water between the capillary and airspace compartments in lung encounters serial barriers: the alveolar epithelium, interstitium, and capillary endothelium. We previously reported a pleural surface fluorescence method to measure net capillary-to-airspace water transport. To measure the osmotic water permeability across the microvascular endothelial barrier in intact lung, the airspace was filled with a water-immiscible fluorocarbon. The capillaries were perfused via the pulmonary artery with solutions of specified osmolalites containing a high-molecular-weight fluorescent dextran. An increase in perfusate osmolality produced a prompt decrease in surface fluorescence due to dye dilution in the capillaries, followed by a slower return to initial fluorescence as capillary and lung interstitial osmolality equilibrate. A mathematical model was developed to determine the osmotic water permeability coefficient (P_f) of lung microvessels from the time course of pleural surface fluorescence. As predicted, the magnitude of the prompt change in surface fluorescence increased with decreased pulmonary artery perfusion rate and increased osmotic gradient size. With raffinose used to induce the osmotic gradient, P_f was 0.03 cm/s at 23°C and was reduced 54% by 0.5 mM $HgCl_2$. Temperature dependence measurements gave an Arrhenius activation energy (E_a) of 5.4 kcal/mol (12–37°C). The apparent P_f induced by the smaller osmolytes mannitol and glycine was 0.021 and 0.011 cm/s (23°C). Immunoblot analysis showed $\sim 1.4 \times 10^{12}$ aquaporin-1 water channels/cm^2 of capillary surface, which accounted quantitatively for the high P_f. These results establish a novel method for measuring osmotically driven water permeability across microvessels in intact lung. The high P_f, low E_a, and mercurial inhibition indicate the involvement of molecular water channels in water transport across the lung endothelium.

INTRODUCTION

Movement of salt and water between the airspace and capillary compartments in the adult lung is important for maintaining proper airspace hydration. In the perinatal lung, fluid movement from airspace to capillary provides the mechanism for absorption of airspace fluid in preparation for alveolar respiration (Bland, 1990; Boucher, 1994). Fluid movement between the interstitial and capillary compartments is particularly important in the formation and resolution of interstitial pulmonary edema (Staub, 1974; Matthay et al., 1996). Although it is generally thought that the alveolar epithelium is the primary barrier to water and solute movement from airspace to capillaries (Wangensteen, 1974), there has been no direct experimental measurement of osmotic water permeability across the alveolar endothelium.

We recently developed methods to measure the water permeability of the composite barrier separating the capillary and airspace compartments in intact lung. The airspace was filled with fluid, and the time course of airspace fluid osmolality was measured in response to osmotic gradients imposed between capillary and airspace fluid. In an initial study in the in situ perfused sheep lung (Folkesson et al., 1994), the vascular compartment was perfused with isosmolar saline (300 mosm), and the airspace was filled with hypertonic saline (900 mosm). Serial measurements of airspace fluid osmolality by intratracheal cannulation showed high osmotic water permeability ($P_f \approx 0.02$ cm/s) that was weakly temperature-dependent and reversibly inhibited by mercurials. For studies in small animals, where rapid airspace fluid instillation and sampling is not practical, a pleural surface fluorescence method was developed in which airspace fluid osmolality was determined from the fluorescence of an indicator dissolved in the airspace fluid (Carter et al., 1996). A capillary-to-airspace osmotic gradient was rapidly established in an isolated lung preparation by changing the osmolality of fluid perfused through the pulmonary artery. The surface fluorescence method was used to demonstrate high osmotic water permeability ($P_f =$ 0.017 cm/s) in mouse lung, and with the use of specific fluorescent indicators, to measure diffusional water permeability and proton/bicarbonate transport. Transport measurements utilizing fluorescent probes in the airspace compartment do not provide information about the individual permeabilities of alveolar epithelial and endothelial barriers.

The purpose of this study was to measure water permeability of the lung microvascular endothelial barrier. An additional motivation for this study was to determine whether molecular water channels (aquaporins) are involved in lung endothelial water permeability. Water channel aquaporin-1 (AQP1, CHIP28) is expressed strongly in lung capillary endothelium (Nielsen et al., 1993; Hasegawa et al., 1994; Folkesson et al., 1994; Schnitzer and Oh, 1996;

Received for publication 11 September 1997 and in final form 12 December 1997.

Address reprint requests to Dr. Alan S. Verkman, Cardiovascular Research Institute, 1246 Health Sciences East Tower, Box 0521, University of California, San Francisco, CA 94143-0521. Tel.: 415-476-8530; Fax: 415-665-3847; E-mail: verkman@itsa.ucsf.edu.

0006-3495/98/04/2121/08 $2.00

Effros et al., 1997) in a developmentally regulated manner (Bondy et al., 1993; Umenishi et al., 1996; King et al., 1996). AQP1 is a mercurial-sensitive, water-selective transporter expressed widely in fluid-transporting epithelia and endothelia (for a review, see Verkman et al., 1996; Lee et al., 1997). If AQP1 facilitates water movement across lung microvessels, then it is predicted that microvascular osmotic water permeability (P_f) should be high, weakly temperature-dependent, and inhibited by mercurials. High P_f mediated by AQP1 would also suggest significant transcellular osmotic water movement across the capillary endothelium.

Our strategy for measuring microvascular endothelial water permeability is depicted in Fig. 1. The airspace was filled with an inert, water-insoluble fluorocarbon to restrict lung water to two principal compartments: an "interstitial compartment" and the flowing capillary compartment. Under these conditions the capillary endothelium becomes the rate-limiting permeability barrier. The pulmonary artery was perfused with solutions of specified osmolalities containing equal concentrations of a high-molecular-weight fluorescent dextran. In response to a change in perfusate osmolality, water was osmotically driven into or out of the capillaries, resulting in fluorophore dilution or concentration, respectively. The resultant change in fluorophore concentration was recorded as a prompt change (decrease for fluorophore dilution) in pleural surface fluorescence. As demonstrated by the model and confirmed experimentally, the magnitude of the deflection was related to the osmotic water permeability. The prompt deflection was followed by a slower return of the fluorescence signal to the original level as interstitial and capillary fluid osmolality equilibrate. The rate of equilibration is related to a combination of water permeability, pulmonary artery flow, and interstitial volume. We report here the development and validation of the method, a mathematical model for determining P_f from fluorescence signals, and a characterization of microvascular water permeability in intact mouse lung.

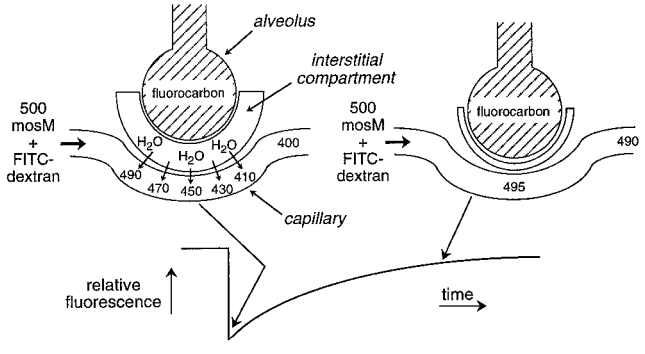

FIGURE 1 Strategy for measuring osmotic water permeability of microvessels in intact lung. The airspace is filled with an inert fluorocarbon, and the pulmonary artery is perfused with solutions of specified osmolalities containing FITC-dextran. Pleural surface fluorescence is monitored continuously by epifluorescence microscopy. In response to an increase in perfusate osmolality, water is extracted from the interstitial space, the capillary fluorophore is diluted, and the pleural surface fluorescence signal decreases. As interstitial and capillary osmolality equilibrate, water movement slows and fluorescence returns to its original level. See text for details.

METHODS

Lung preparation

The isolated perfused lung preparation was described previously in detail (Carter et al., 1996). c57 mice (20–25 g weight; Benton-Kingman, Freemont, CA) were euthanized with intraperitoneal pentobarbital (150 mg/kg). The trachea was cannulated in situ with polyethylene PE-50 tubing. The airspace was filled with 0.3–0.5 ml of Fluorinert (3M, St. Paul, MN), an inert fluorocarbon that is immiscible with water and remains confined to the airspace compartment. The pulmonary artery and left atrium were transected, and the pulmonary artery was cannulated with PE-20 tubing. The heart and lungs were moved en bloc to a Lucite perfusion chamber for observation by epifluorescence microscopy. One lung was positioned above a narrow channel in which phosphate-buffered saline (PBS) (pH 7.4, 300 mosm) was continuously perfused (10–20 ml/min) between the external pleural surface and the coverglass. The pulmonary artery was gravity perfused at constant pressure (25–35 cm H_2O) with a four-way flow valve to select solutions. The pulmonary artery was initially perfused with HEPES-buffered Ringer's (HBR) (137 mM NaCl, 2.68 mM KCl, 1.25 mM $MgSO_4$, 1.82 mM $CaCl_2$, 5.5 mM glucose, 12 mM HEPES, 1.5% bovine serum albumin; pH 7.4; 300 mosm) for 5 min to remove all blood, and to set the reservoir height for the desired perfusion rate (generally 1–2.5 ml/min). The temperature of the pulmonary artery and pleural surface perfusates was controlled by circulating water around the perfusion inflow tubing.

Pleural surface fluorescence microscopy

The fluorescence intensity from a ~5-mm-diameter spot on the lung pleural surface was monitored with an inverted epifluorescence microscope (Nikon Diaphot). The spot was illuminated with a tungsten-halogen lamp in series with a neutral density filter (optical density 1.0), an interference filter (480 ± 5 nm), and a dichroic mirror (510 nm). A 10× dry objective (Leitz, numerical aperture 0.25) was used for all measurements. Emitted fluorescence was filtered with a cut-on filter (> 515 nm) and detected with a photomultiplier. The photomultiplier signal was amplified, digitized at 30 Hz by a 12-bit analog-to-digital converter, and binned in 1-s time intervals. There was no photobleaching at the low illumination intensity used here.

Lung microvascular osmotic water permeability

Water movement across lung microvessels was measured by perfusing lungs with fluorescent solutions of specified osmolalities. Solutions consisted of HBR (300 mosm) with 100–300 mM osmolyte (glycine, mannitol, sucrose, or raffinose) and fluorescein isothiocyanate-dextran (FITC-dextran) (0.5 mg/ml, 500 kDa; Sigma). The FITC-dextran was passed through a PD-10 size exclusion column (Pharmacia Biotech, Uppsala, Sweden) before measurements to remove any unconjugated FITC. Fluorescence intensities were identical in the isosmolar and hyperosmolar HBR solutions. As described in reference to Fig. 1, osmotic water movement was measured from the time course of fluorescence in response to switching the perfusate between HBR + FITC-dextran (300 mosm) and hyperosmolar HBR + FITC-dextran (400–600 mosm). In the studies of water transport inhibition, the capillaries were lightly fixed by a 15-s perfusion with HBR containing 1% glutaraldehyde, and then perfusate osmolalities were changed in the absence and presence of $HgCl_2$. Osmotic water permeability coefficients (P_f) were determined with a mathematical model described below. Fluorescence time course data were fitted to a biexponential function [$F(t) = a_o + a_1 e^{-b_1 t} + a_2 e^{-b_2 t}$] to determine the amplitude of the initial deflection in fluorescence signal (a_1) and the time constant for the phase of slower recovery ($1/b_2$).

Immunoblot analysis

Lungs from euthanized mice were immediately harvested, homogenized in PBS containing protease inhibitors at 4°C, and dissolved in SDS loading buffer. Protein was determined by the Bradford assay. Lung homogenates and purified AQP1 protein standards (Van Hoek and Verkman, 1992) were electrophoresed on a 12% SDS-polyacryamide gel and electroblotted onto a polyvinylidene difluoride membrane. The membrane was incubated with a 1:1000 dilution of anti-AQP1 immune serum. Blots were washed in PBS, incubated with an alkaline phosphatase-conjugated goat anti-rabbit IgG antibody (1:3000; Life Technologies), and developed with 5-bromo-4-chloro-3-indolyl-phosphate (16 μg/ml) and nitroblue tetrazolium (0.33 μg/ml) separately by enhanced chemiluminescence.

Mathematical model

Fig. 2 shows a schematic of the two-compartment model consisting of an interstitial space in contact with a flowing capillary compartment. The interstitial space is defined by a volume $V_i(t)$ and an osmolality $\phi_i(t)$. The capillary compartment is defined by a local axial volume flow rate $f(x, t)$ (in cm^3/s) and a local osmolality $\phi_c(x, t)$. The parameters $V_i(0)$, $f(0, t)$, $\phi_i(0)$, and $\phi_c(0, t)$, along with single capillary length (L, cm) and surface area (S, in cm^2/cm length), are specified to compute $f(x, t)$ as described below. It is assumed that only water moves between compartments.

By definition, volume flow across the capillary-interstitial barrier is given by $J_v = P_f S v_w [\phi_c(x, t) - \phi_i(t)]$, where J_v is volume flow in cm^2/s (cm^3/s per cm length) and v_w is the partial molar volume of water (18 cm^3/mol). Recognizing that $\phi_i(0)V_i(0) = \phi_i(t)V_i(t)$ and $f(0, t)\phi_c(0, t) = f(x, t)\phi_c(x, t)$,

$$J_v(x, t) = P_f S v_w[\phi_c(0)f(0, t)/f(x, t) - \phi_i(0)V_i(0)/V_i(t)] \quad (1)$$

The flow of volume out of the interstitial compartment results in a decrease in $V_i(t)$,

$$-dV_i(t)/dt = \int_0^L J_v(x, t)dx \quad (2)$$

As volume enters the flowing capillary compartment, axial volume flow $f(x, t)$ increases,

$$df(x, t)/dx = J_v(x, t) \quad (3)$$

Equations 1–3 were solved numerically to give the axial volume flow rate along the capillary, $f(x, t)$. The step sizes for the numerical solution were $\Delta x = L/100$ and $\Delta t = \Delta x/v_c$, where v_c is the initial flow velocity (cm/s) in the capillary computed from initial flow rate and capillary radius. In the initial phase of the calculation, before the anisomolar perfusate traverses the full capillary length, the equations were solved only for the portion of the capillary that has been in contact with the new perfusate (determined from v_c and time). The model assumed that diffusion of osmolytes along the capillary length does not occur, that the interstitial compartment is well mixed, and that the capillary geometry remains constant. In addition, it is noted that subpleural surface vessels are representative of vessels in other regions of the lung, and that alveolar capillaries and small exchanging arterioles and venules comprise >90% of lung blood volume (McLaughlin et al., 1961).

The measured pleural surface fluorescence signal relative to that before a change in perfusate osmolality, $F(t)/F_o$, is given by

$$F(t)/F_o = (1/L)\int_0^L f(0, t)/f(x, t)dx \quad (4)$$

Parameter selection

P_f and $V_i(0)$ are fitted parameters determined from the experimental data. The osmolalities $\phi_i(0)$ and $\phi_c(0, t)$ are specified experimentally. Morphometric measurements of mouse lung indicated a total (per two lungs) capillary volume of 0.084 cm^3 and a surface area of 590 cm^2 (Geelhaar and Weibel, 1971). Assuming a circular capillary profile, these values yield a capillary diameter of 5.7 μm and a total capillary length of 3.4×10^5 cm, giving a value of parameter S of 0.0018 cm^2/cm. Capillary flow $f(0, t)$ was computed to be $(2.7 \times 10^{-9})f_p$ cm^3/s, where f_p is pulmonary artery perfusate flow rate in ml/min; this value was based on a capillary flow velocity of 0.085 cm/s (Johnson et al., 1960; Kuhnle et al., 1993) at a normal mouse cardiac output of 13 cm^3/min (Wang et al., 1993). The average capillary length L was assumed to be 0.01 cm, based on comparative measurements in mammalian lungs (Staub and Schultz, 1968) and data from rabbit lung (Schlosser et al., 1965). Because of uncertainties in available data for the value of L, computations were done for a range of possible L from 0.005 to 0.02 cm (see Fig. 4 *C*).

RESULTS

Fig. 3 shows a pleural surface fluorescence measurement in which the airspace of the lung was filled with an inert fluorocarbon and the pulmonary artery was perfused at 1.7

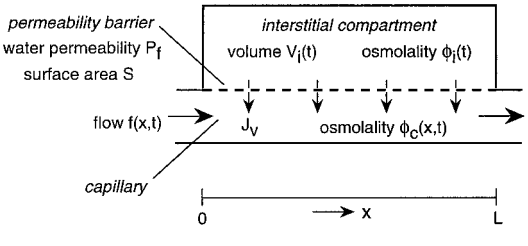

FIGURE 2 Two-compartment model of osmotic water transport across lung microvessels. The interstitial compartment is modeled as a well-mixed space of variable volume in contact with the flowing capillary compartment. The capillary endothelium is taken as a single, rate-limiting water-permeable barrier (*dashed line*) separating the compartments. Parameters: P_f, osmotic water permeability (cm/s); $V_i(t)$, interstitial volume (cm^3); $f(x, t)$, capillary lumen flow (cm^3/s); $\phi_c(x, t)$, capillary lumen osmolality (mosm); $\phi_i(t)$, interstitial osmolality (mosm); L, capillary length (cm); S, capillary surface area per unit length (cm^2/cm).

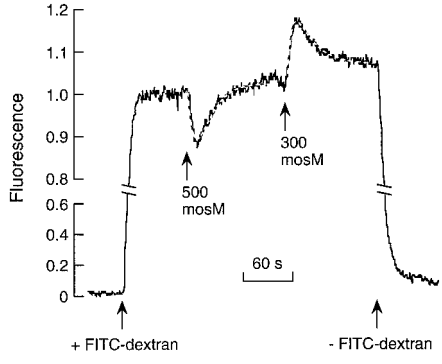

FIGURE 3 Time course of pleural surface fluorescence in response to changes in perfusate osmolality. The airspace was filled with an inert fluorocarbon and the pulmonary artery perfused with HBR (300 mosm) or HBR containing 200 mM raffinose (500 mosm), each containing 0.5 mg/ml FITC-dextran (500 kDa). Perfusate flow was 1.7 ml/min at 23°C. Fitted biexponential functions are shown (*dashed curves*).

ml/min with isosmolar (300 mosm) or hyperosmolar (500 mosm) solutions, each containing 0.5 mg/ml of FITC-dextran (500 kDa). There was <1% background signal before addition of FITC-dextran. Upon switching from HBR to HBR containing FITC-dextran, fluorescence increased rapidly, with a $t_{1/2}$ of 3–5 s, indicating adequacy of the perfusion. Increasing perfusate osmolality to 500 mosm (using 200 mM raffinose as osmolyte) without changing the solution fluorescence (same FITC-dextran concentration) produced a prompt decrease in fluorescence followed by a slower return to near-initial values. Return of solution osmolality to 300 mosm produced a prompt deflection in the opposite direction followed by a slower return. The fluorescence returned to near zero upon perfusion with HBR (not containing FITC-dextran) at the end of the experiment, indicating no detectable leakage of FITC-dextran into the lung interstitium. These results are consistent with the theoretical expectations in Fig. 1. To estimate the relative amplitudes of the prompt deflections ($\Delta F/F$) and the half-time ($t_{1/2}$) for the slower return phase, the data were fitted to biexponential functions, as shown by the dashed curves in Fig. 3. In 12 measurements in separate lungs studied by the protocol in Fig. 3, the average prompt deflection $\Delta F/F$ was 0.13 ± 0.02 (SE) and $t_{1/2}$ was 18 ± 4 s. At the end of the experiment, withdrawal of fluid through the tracheal cannula recovered the fluorocarbon without contaminating water. However, in some experiments (<10%) there was lung damage in which the fluorocarbon leaked into the perfusate and/or water leaked into the airspaces; these lungs were discarded. Also, in some experiments the slower phase of the fluorescence response did not return the signal to the initial level, probably because of a reversible change in capillary caliber related to changes in interstitial pressure.

The mathematical model was used to relate $\Delta F/F$ to water permeability coefficient P_f. Fig. 4 shows predictions of the model utilizing parameters for mouse lung. Fig. 4 *A* shows the time course of fluorescence as a function of P_f and interstitial volume V_i. The model predicts a prompt signal deflection whose magnitude depends on P_f, followed by an increase in fluorescence to its initial level. The area between the 1.0 relative fluorescence line and the predicted recovery curve is related to interstitial volume. Comparison of the data in Fig. 3 with the model gives a P_f of 0.03 cm/s and a V_i of 7×10^{-8} cm^3. It is noted that V_i should be considered an apparent volume because the model did not take into account complexities such as osmolyte diffusion and microvascular heterogeneity. For these P_f and V_i values, Fig. 4 *B* compares the predicted time course of fluorescence with the time course of interstitial volume and the flow profile along the capillary axis. As expected, return of the fluorescence signal is associated with equilibration of interstitial volume over a similar time course. Volume flow increases along the capillary axis as water moves from the interstitium into the capillary lumen. The axial changes in flow are greatest at early times where osmotically driven water flow is maximal. Axial volume flow at 0.6 s levels off because the hyperosmolar front has not traversed the full capillary length. Importantly, the flow profiles indicate that flow does not become constant by the end of the capillary, indicating that microvascular P_f is not "flow-limited" under the exper-

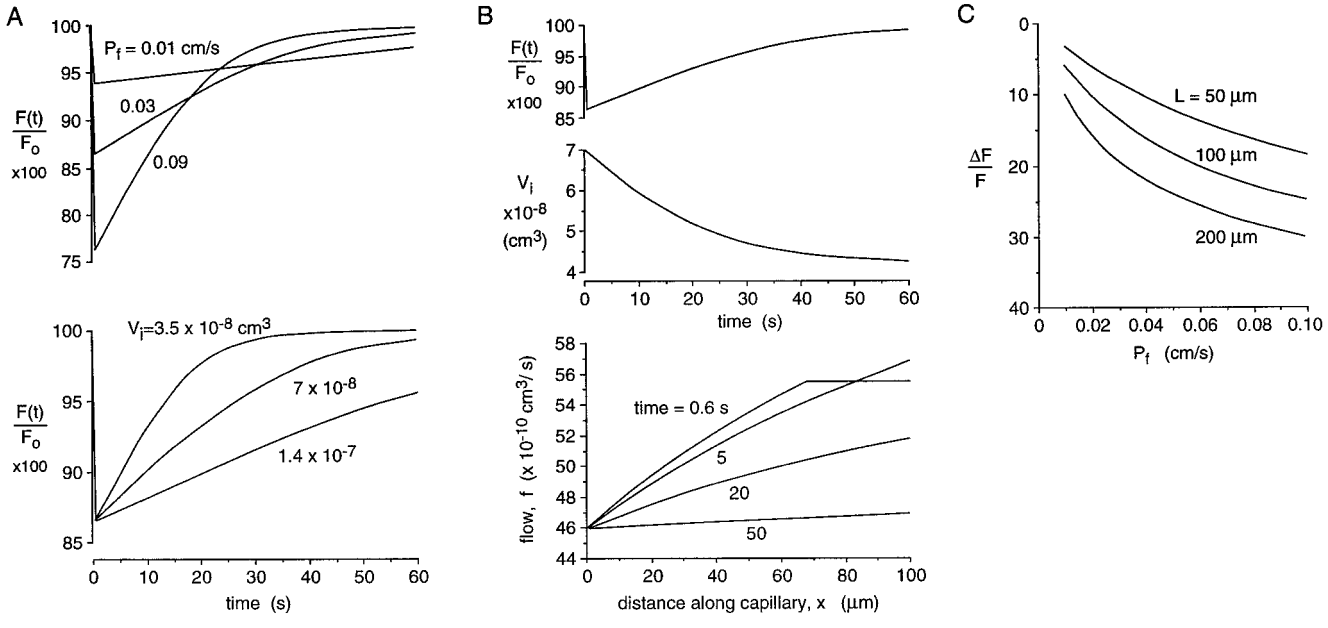

FIGURE 4 Predictions of the mathematical model for determination of microvascular osmotic water permeability. Equations 1–4 were solved numerically as described in Methods. (*A*) Dependence of fluorescence time course on P_f and V_i. Parameters: $\phi_i(0) = 300$ mosm, $\phi_c(x, 0) = 500$ mosm, $S = 0.0018$ cm^2/cm, $L = 0.01$ cm, $f(x, 0) = 4.6 \times 10^{-9}$ cm^3/s, $V_i = 7 \times 10^{-8}$ cm^3 (*top*), $P_f = 0.03$ cm/s (*bottom*). (*B*) Time course of fluorescence, V_i, and axial volume flow, *f*. Parameters are as in *A*, with $P_f = 0.03$ cm/s and $V_i = 7 \times 10^{-8}$ cm^3. (*C*) Empirical relationship between $\Delta F/F$ and P_f for different values of capillary length *L*.

imental conditions. Fig. 4 *C* shows the deduced empirical relationship between $\Delta F/F$ and P_f for different capillary lengths. Similar plots (computed with appropriate parameters) were used to deduce P_f values for the experimental maneuvers below.

Experiments were carried out to test model predictions and to characterize lung microvascular water permeability. Fig. 5 *A* shows that the prompt signal deflection $\Delta F/F$ increases in an approximately linear manner with the size of the osmotic gradient. Corresponding P_f values were very high: 0.034, 0.031, and 0.028 cm/s (23°C) for the gradients of 100, 200, and 300 mosm, respectively. Fig. 5 *B* shows that $\Delta F/F$ decreases with increasing perfusion flow rates, as predicted theoretically. For the same osmotic gradient, increasing flow produces less signal change (decreased $\Delta F/F$), because more volume is presented to attenuate the change in FITC-dextran concentration.

The Arrhenius activation energy (E_a), which is determined from the temperature-dependence of water permeability, is a useful parameter for characterizing the water permeation pathway; E_a is generally >8–10 kcal/mol for water movement through a lipid bilayer and <6 kcal/mol for water movement through an aqueous pore such as a molecular water channel (Finkelstein, 1987). Fig. 5 *C* (*top*) shows that increasing temperature produced a greater signal deflection, indicating higher water permeability. The Arrhenius plot (Fig. 5 *C*, *bottom*) relating $\ln(\Delta F/F)$ to reciprocal absolute temperature indicates an apparent E_a (model independent) of 5.4 ± 1 kcal/mol. This apparent E_a is similar to that of 5.2 kcal/mol determined from an Arrhenius plot of $\ln(P_f)$ versus $1/T$, where P_f values were deduced from $\Delta F/F$ by using the model. The low E_a suggests the involvement of molecular water channels.

As described in the Introduction, lung capillary endothelial cells express AQP1, a mercurial-sensitive water-transporting protein. AQP1-mediated water permeability in erythrocytes and various heterologous expression systems is inhibited by mercurials such as $HgCl_2$. Initial studies with $HgCl_2$ (0.1–0.5 mM) in the perfusate produced marked lung damage, resulting in unacceptable fluorocarbon and FITC-dextran leakage. To study the $HgCl_2$ effect, we used a strategy initially developed to study mercurial inhibition in intact tissues such as frog urinary bladders (Ibarra et al., 1989) and perfused renal vasa recta (Pallone et al., 1997). Lungs were lightly fixed with glutaraldehyde before measurement of water permeability. This maneuver did not affect capillary P_f (Fig. 6 *A*, *right*), in agreement with findings in the bladder and vasa recta. Fig. 6 *A* (*left*) shows an original experimental tracing, where signal amplitude was decreased (indicating water transport inhibition) when $HgCl_2$ was present in the perfusate. The averaged data summarized in Fig. 6 *A* (*right*) indicate water transport inhibition by 36% and 54% for $HgCl_2$ concentrations of 0.3 and 0.5 mM, respectively.

Water transport was induced by osmolytes of different size to determine whether osmolyte reflection coefficient was size-dependent and less than unity. Fig. 6 *B* (*left*) shows an experiment in which water transport was induced by 200 mM gradients of raffinose (M_r 594 Da) and then glycine (75 Da). Fig. 6 *B* (*right*) summarizes $\Delta F/F$ values for osmolytes of different sizes, showing a small but significant dependence of the magnitude of the induced water permeability on osmolyte size (see Discussion).

The AQP1 water channel is primarily expressed in capillary endothelial cells in lung. Quantitative immunoblot analysis was done to determine the amount of AQP1 per lung and to estimate whether the amount of AQP1 is adequate to account for the measured high P_f values. Fig. 7 shows an immunoblot of total lung homogenate from three mice, along with purified AQP1 protein standards. Quantitative densitometry indicated the expression of 41 ± 6 μg AQP1 protein per two mouse lungs. Assuming a total capillary length of 3.4×10^5 cm (see above) and that essentially all AQP1 is in capillary endothelia, this value corresponds to a density of $\sim 1.4 \times 10^{12}$ AQP1 monomers/cm^2 of endothelial cell plasma membrane. Given a single-chan-

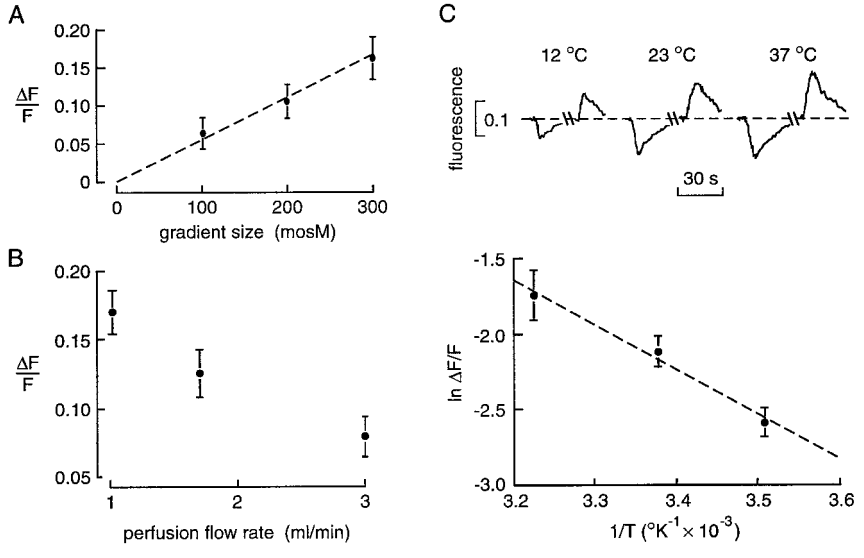

FIGURE 5 Experimental test of model predictions. (*A*) Dependence of the magnitude of the prompt deflection in pleural surface fluorescence ($\Delta F/F$, SE) on osmotic gradient size. Perfusates consisted of HBR containing 0 or 200 mM raffinose. Perfusate flow rate was 1.7 ml/min. (*B*) Dependence of $\Delta F/F$ on perfusate flow. The perfusate consisted of HBR with 300 mM raffinose (500 mosm). (*C*) Temperature dependence. *Top*: Representative time course data (conditions as in Fig. 3) at indicated temperatures. *Bottom*: Arrhenius plot (SE, three to five lung perfusions) with fitted activation energy (E_a) of 5.4 ± 1 kcal/mol.

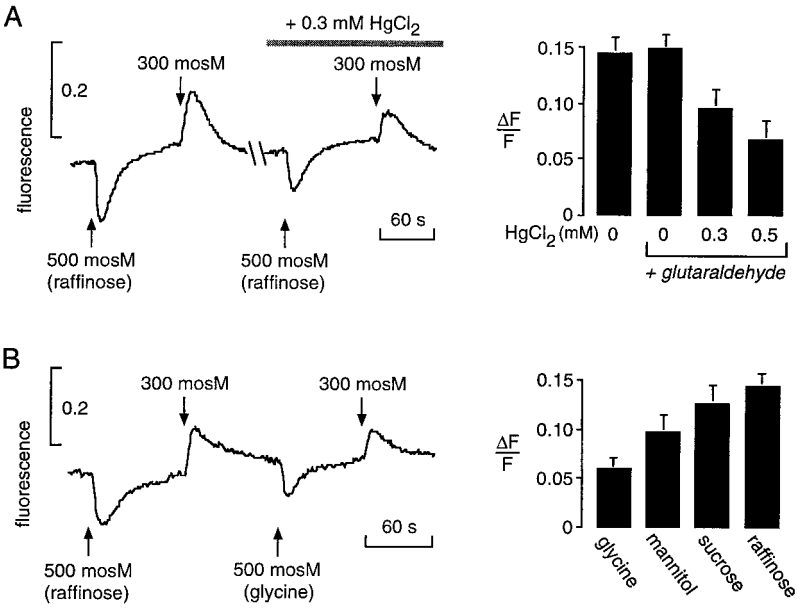

FIGURE 6 Characterization of microvascular endothelial water permeability. (*A*) Inhibition of water permeability by $HgCl_2$. *Left*: Representative fluorescence time course data. Lungs were lightly fixed for 15 s with 1% glutaraldehyde in cacodylate buffer (300 mosm, pH 7.4) and then perfused with HBR or HBR + 200 mM raffinose. The perfusate flow rate was 1.7 ml/min, 23°C. Where indicated, 0.3 mM $HgCl_2$ was present in the solutions. *Right*: Average (SE, three to five independent lung perfusions) $\Delta F/F$, showing effect of glutaraldehyde fixation and $HgCl_2$. (*B*) Effect of osmolyte size on fluorescence time course. *Left*: Representative fluorescence time course. Solutions contained HBR and 200 mM raffinose or glycine with perfusate flow rate 1.7 ml/min, 23°C. *Right*: Averaged $\Delta F/F$ (SE, three to five lung perfusions) for osmotic gradients with indicated solutes.

nel AQP1 water permeability of 10^{-13} cm^3/s at 23°C (Van Hoek and Verkman, 1992), this density predicts an endothelial cell plasma membrane P_f of 0.07 cm/s, and a transendothelial cell P_f of 0.035 cm/s. Notwithstanding the assumptions in the computation, this value is in good agreement with measured P_f.

DISCUSSION

The purpose of this study was to develop a quantitative method of characterizing osmotic water permeability of the intact microvascular endothelial barrier in lung. The blood-gas barrier in the lung comprises serial permeability barriers: the alveolar epithelium, the interstitium, and the capillary endothelium. The pleural surface fluorescence method developed here permits the noninvasive measurement of rapid water movement across alveolar capillaries in intact lung. The lung perfusion method is applicable to lungs of different sizes, such as the perinatal lung in development (Carter et al., 1997). A principal finding here was that lung

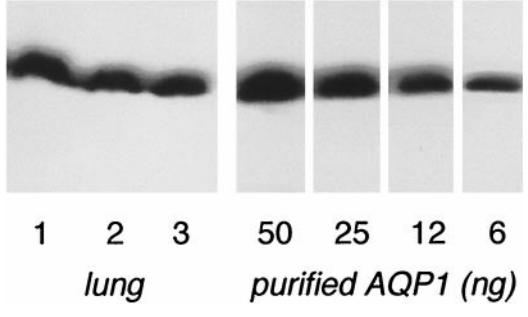

FIGURE 7 AQP1 immunoblot analysis of mouse lung. The total homogenate from three mouse lungs was resolved by SDS-PAGE (10 μg protein/lane) and blotted as described in Methods. Standards consist of purified AQP1 with amounts indicated.

microvascular water permeability has the characteristics of channel-mediated water permeability (Finkelstein, 1987; Verkman et al., 1996): a high water permeability coefficient that is weakly temperature-dependent and is inhibited by mercurials.

The high P_f of 0.03 cm/s at 23°C (0.045 cm/s at 37°C) formally represents a lower limit to microvascular endothelial water permeability. The mathematical model developed to compute P_f from fluorescence data assumes a single rate-limiting barrier and a perfectly mixed interstitial compartment. Although the rapid signal deflection in response to a change in perfusate osmolality supports this assumption, the rate-limiting barrier may contain contributions from an interstitial resistance to water movement as well as a membrane resistance, arising in part from the basolateral membrane of type I alveolar epithelial cells. The latter component probably represents a minimal resistance to water flow because plasma membrane water permeability in type I cells has been measured to be exceptionally high (0.08 cm/s; Dobbs et al., 1998). Another consideration is that not all of the capillary surface may effectively contact the interstitial space, because of capillary-capillary contact and other ineffective contact geometries. A third factor discussed below is the nonunity reflection coefficient of small osmolytes. However, despite these factors, which would each increase P_f, the measured P_f is already substantially higher than the P_f of 0.017 measured for the composite airspace-capillary barrier in mouse lung (Carter et al., 1996). The microvascular capillary endothelium is therefore not a major rate-limiting barrier for osmotically driven water movement between the airspace and capillary compartments.

Previous measurements have been reported for water transport across endothelial cells from pulmonary artery and renal vasa recta. Osmotic (P_f) and diffusional (P_d) water permeabilities in isolated pulmonary artery endothelial cells

increased from 0.0016 cm/s at 20°C to 0.0035 cm/s at 41°C (Garrick, 1988a,b). The low permeability values and similar P_f and P_d suggested the absence of functional water channels in the pulmonary artery endothelial preparation. A recent measurement of transendothelial water transport in isolated perfused descending vasa recta of kidney showed very high P_f (0.12 cm/s) that was strongly inhibited by the mercurial pCMBS (Pallone et al., 1997). As found for the alveolar capillary endothelia, descending vasa recta endothelia express large amounts of AQP1 protein.

Two studies have addressed water permeability across microvascular endothelia in lung. In isolated perfused rat and dog lungs, the permeabilities of the endothelium to antipyrine and ^3H_2O were estimated by indicator dilution (Cua et al., 1990). Capillary P_d was 5.8×10^{-5} cm/s at 21°C and 6.4×10^{-5} cm/s at 38°C. These low values indicate that ^3H_2O is "flow-limited," and that true capillary P_d is greatly underestimated because of unstirred layers. A similar conclusion regarding unstirred layers was reported in isolated perfused distal airways, based on low P_d values (0.5×10^{-5} cm/s) (Folkesson et al., 1996). Recently, Effros et al. (1997) measured the clearances of ^3H_2O and unlabeled water in rat lungs by collection of pulmonary venous perfusates. Although the clearance of ^3H_2O was found to flow-limited, the clearances of ^3H_2O and unlabeled water were partially inhibited by $HgCl_2$. Absolute P_f values were not reported because of the limited time resolution of the fluid collections, as well as uncertainties in surface areas and the location of rate-limiting barriers. The results here provide the first determination of P_f of the lung microvascular endothelium and indicate that this endothelium is similar to the renal vasa recta in terms of its water permeability properties.

Immunocytochemistry indicates that the primary water channel present in the pulmonary capillary endothelium is AQP1 (Nielsen et al., 1993; Hasegawa et al., 1994; Folkesson et al., 1994; Schnitzer and Oh, 1996; Effros et al., 1997). The quantitative immunoblot data provided in this study demonstrate the expression of substantial amounts of AQP1 protein in mouse lung. As described in the Results, the density of AQP1 monomers in endothelial cell plasma membranes is $\sim 1.4 \times 10^{12}/cm^2$ of membrane, predicting a very high plasma membrane P_f of ~0.07 cm/s at 23°C. For water movement across two such plasma membranes in the intact endothelium, P_f would be ~0.035 cm/s. This value is just larger than that of 0.03 cm/s for the capillary endothelium measured here. Differences may be related to many factors, including uncertainties in capillary surface area, underestimation of true microvascular P_f as described above, and nonzero interstitial resistances to water flow. In addition, there is a possibility that other as yet unidentified water channels contribute to microvascular water permeability. Water permeability measurements in knockout mice lacking AQP1 water channels will be needed to evaluate this possibility.

It was found that the magnitude of osmotically induced water movement depends on osmolyte size. In terms of classical nonequilibrium thermodynamics, the data suggest that the apparent reflection coefficients for mannitol and glycine are less than unity. The reflection coefficients for raffinose and sucrose may also be less than 1; however, it was not possible to study osmolytes larger than raffinose because of difficulties in dissolving such compounds at concentrations greater than 100 mM and measuring their osmolalities accurately. It is noted that some diffusion of small osmolytes out of capillaries might occur under the conditions of our experiments. Nonzero osmolyte diffusion is predicted to affect mainly the slower phase of the fluorescence signal; however, the interpretation of low reflection coefficients for small solutes must be made cautiously if substantial solute diffusion occurs across some microvessels. Because AQP1 is a water-selective transporter that does not pass even small molecules, a reflection coefficient under unity for small solutes indicates both transcellular and paracellular routes for water movement. Similar conclusions were reported for water movement in vasa recta endothelia (Pallone et al., 1990, 1997). In contrast, rates of water transport between the airspace and capillary compartments did not depend on the size of the osmolyte added to the airspace compartment (Carter et al., 1996), suggesting little paracellular water transport across the alveolar epithelium. In the older literature (Taylor and Gaar, 1970; Perl et al., 1975), low solute reflection coefficients were reported for the endothelium in isolated dog lung by following changes in lung weight in response to the addition of solutes to the pulmonary artery perfusate. It is difficult to compare the data here with results from these older studies because of uncertainties in deducing the rates of water and solute movement across lung microvessels from serial whole lung weight determinations.

It is noted that the measurements of temperature dependence, $HgCl_2$ inhibition, and osmolyte size are comparative, so that conclusions do not depend on the details of the mathematical model. However, the determination of absolute P_f required modeling. The alveolar-capillary geometry is complex in that several capillaries serve each larger alveolus and each capillary serves several alveoli. At any point along its length, a capillary is bordered by an alveolus on two sides, with a relatively small interstitial space separating the two compartments. These considerations indicated the modeling of an individual capillary enclosed by a rate-limiting barrier through which osmotically driven water transport occurs. Possible heterogeneity in the effective length per capillary could not be taken into account because of the paucity of data on this issue. Fortunately, a substantial body of morphometric data on other aspects of the lung capillary endothelium was available, especially in the older literature. The parameters corresponding to capillary volume, surface area, and flow were chosen from well-established values. The greatest uncertainty was in the selection of capillary length, where values from 0.007 to 0.02 cm have been reported. We chose a reasonable intermediate value (0.01 cm); the model indicated a variation in P_f from

0.013 to 0.046 cm/s for the extreme values of capillary length.

In summary, the results here establish a simple biophysical method for measuring rapid microvascular osmotic water permeability in mammalian lung. Quantitative water transport measurements in intact organs should be very useful in the phenotype analysis of transgenic mice lacking specific aquaporins (Ma et al., 1997, 1998). The high microvascular water permeability suggests that alveolar capillaries do not constitute a rate-limiting barrier in lung water movement. The specific water permeability properties suggest the involvement of molecular water channels in the high transcellular endothelial water permeability in lung microvessels.

We thank Dr. Baoxue Yang for help in the immunoblot analysis and Dr. Richard Effros for advice and suggestions.

This work was supported by grants HL51854, DK35124, DK43840, and HL42368 from the National Institutes of Health, and grant R613 from the National Cystic Fibrosis Foundation. EPC was supported by a fellowship from the American Lung Association.

REFERENCES

Bland, R. D. 1990. Lung epithelial ion transport and fluid movement during the perinatal period. *Am. J. Physiol.* 259:L30–L37.

Bondy, C., E. Chin, B. L. Smith, G. M. Preston, and P. Agre. 1993. Developmental gene expression and tissue distribution of the CHIP28 water-channel protein. *Proc. Natl. Acad. Sci. USA.* 90:4500–4504.

Boucher, R. C. 1994. Human airway ion transport. Part one. *Am. J. Respir. Crit. Care Med.* 150:271–281.

Carter, E. P., M. A. Matthay, J. Farinas, and A. S. Verkman. 1996. Transalveolar osmotic and diffusional water permeability in intact mouse lung measured by a novel surface fluorescence method. *J. Gen. Physiol.* 108:133–142.

Carter, E. P., F. Umenishi, M. A. Matthay, and A. S. Verkman. 1997. Developmental changes in alveolar water permeability in perinatal rabbit lung. *J. Clin. Invest.* 100:1071–1078.

Cua, W. O., G. Basset, F. Bouchonnet, R. A. Garrick, G. Saumon, and F. P. Chinard. 1990. Endothelial and epithelial permeabilities to antipyrine in rat and dog lungs. *Am. J. Physiol.* 258:H13210–H1333.

Dobbs, L., R. Gonzalez, M. A. Matthay, E. P. Carter, and A. S. Verkman. 1998. Highly water-permeable type I alveolar epithelial cells confer high transalveolar water permeability in rat lung. *Proc. Natl. Acad. Sci. USA.* In press.

Effros, R. M., C. Darin, E. R. Jacobs, R. A. Rogers, G. Krenz, and E. E. Schneeberger. 1997. Water transport and distribution of aquaporin-1 in the pulmonary airspaces. *J. Appl. Physiol.* 83:1002–1016.

Finkelstein, A. 1987. Water Movement Through Lipid Bilayers, Pores and Plasma Membranes: Theory and Reality. John Wiley and Sons, New York.

Folkesson, H., M. Matthay, A. Frigeri, and A. S. Verkman. 1996. High transepithelial water permeability in microperfused distal airways: evidence for channel-mediated water transport. *J. Clin. Invest.* 97:664–671.

Folkesson, H. G., M. A. Matthay, H. Hasegawa, F. Kheradmand, and A. S. Verkman. 1994. Transcellular water transport in lung alveolar epithelium through mercury-sensitive water channels. *Proc. Natl. Acad. Sci. USA.* 91:4970–4974.

Garrick, R. A., D. J. DiRisio, R. Giannuzzi, W. O. Cua, U. S. Ryan, and F. P. Chinard. 1988a. The osmotic permeability of isolated calf pulmonary artery endothelial cells. *Biochim. Biophys. Acta.* 939:343–348.

Garrick, R. A., U. S. Ryan, and F. P. Chinard. 1988b. Water permeability of isolated endothelial cells at different temperatures. *Am. J. Physiol.* 255:C311–C314.

Geelhaar, A., and E. R. Weibel. 1971. Morphometric estimation of pulmonary diffusion capacity. *Respir. Physiol.* 11:354–366.

Hasegawa, H., S. C. Lian, W. E. Finkbeiner, and A. S. Verkman. 1994. Extrarenal tissue distribution of CHIP28 water channels by in situ hybridization and antibody staining. *Am. J. Physiol.* 266:C893–C903.

Ibarra, C., P. Ripoche, and J. Bourguet. 1989. Effect of mercurial compounds on net water transport and intramembrane particle aggregates in ADH-treated frog urinary bladder. *J. Membr. Biol.* 110:115–126.

Johnson, R. L., W. S. Spicer, J. M. Bishop, and R. E. Forster. 1960. Pulmonary capillary blood volume, flow, and diffusing capacity during exercise. *J. Appl. Physiol.* 15:893–902.

King, L. S., S. Nielsen, and P. Agre. 1996. Aquaporin-1 water channel protein in lung ontogeny, steroid-induced expression, and distribution in rat. *J. Clin. Invest.* 97:2183–2191.

Kuhnle, G. E. H., F. H. Leipfinger, and A. E. Goetz. 1993. Measurement of microhemodynamics in the ventilated rabbit lung by intravital fluorescence microscopy. *J. Appl. Physiol.* 74:1462–1471.

Lee, M. D., L. S. King, and P. Agre. 1997. The aquaporin family of water channel proteins in clinical medicine. *Rev. Mol. Med.* 76:141–156.

Ma, T., B. Yang, A. Gillespie, E. J. Carlson, C. J. Epstein, and A. S. Verkman. 1997. Generation and phenotype of a transgenic knock-out mouse lacking the mercurial-insensitive water channel aquaporin-4. *J. Clin. Invest.* 100:957–962.

Ma, T., B. Yang, A. Gillespie, E. J. Carlson, C. J. Epstein, and A. S. Verkman. 1998. Severely impaired urinary concentrating ability in transgenic mice lacking aquaporin-1 water channels. *J. Biol. Chem.* 273: 4296–4299.

Matthay, M. A., H. Folkesson, and A. S. Verkman. 1996. Salt and water transport across alveolar and distal airway epithelia in the adult lung. *Am. J. Physiol.* 270:L487–L503.

McLaughlin, R. F., W. S. Tyler, and R. O. Canada. 1961. A study of subgross pulmonary anatomy in various mammals. *J. Am. Med. Assoc.* 175:148–158.

Nielsen, S., B. L. Smith, E. I. Christensen, and P. Agre. 1993. Distribution of the aquaporin CHIP in secretory and resorptive epithelia and capillary endothelia. *Proc. Natl. Acad. Sci. USA.* 90:7275–7279.

Pallone, T. L., B. K. Kishore, S. Nielsen, P. Agre, and M. A. Knepper. 1997. Evidence that aquaporin-1 mediates NaCl-induced water flux across descending vasa recta. *Am. J. Physiol.* 272:F587–F596.

Pallone, T. L., J. Work, and R. L. Jamison. 1990. Resistance of descending vasa recta to the transport of water. *Am. J. Physiol.* 259:F688–F697.

Perl, W., P. Chowdhury, and F. P. Chinard. 1975. Reflection coefficients of dog lung endothelium to small hydrophilic solutes. *Am. J. Physiol.* 228:797–809.

Schlosser, D., E. Heyse, and H. Bartels. 1965. Flow rate of erythrocytes in the capillaries of the lung. *J. Appl. Physiol.* 20:110–112.

Schnitzer, J. E., and P. Oh. 1996. Aquaporin-1 in plasma membrane and caveolae provides mercury-sensitive water channels across rat lung endothelium. *Am. J. Physiol.* 270:H416–H422.

Staub, N. C. 1974. Pulmonary edema. *Physiol. Rev.* 54:678–811.

Staub, N. C., and E. L. Schultz. 1968. Pulmonary capillary length in dog, cat, and rabbit. *Respir. Physiol.* 5:371–378.

Taylor, A. E., and K. A. Gaar. 1970. Estimation of equivalent pore radii of pulmonary capillary and alveolar membranes. *Am. J. Physiol.* 218: 1133–1140.

Umenishi, F., E. P. Carter, B. Yang, B. Oliver, M. A. Matthay, and A. S. Verkman. 1996. Sharp increase in rat lung water channel expression in the perinatal period. *Am. J. Respir. Cell Mol. Biol.* 15:673–679.

Van Hoek, A. N., and A. S. Verkman. 1992. Functional reconstitution of the isolated erythrocyte water channel CHIP28. *J. Biol. Chem.* 267: 18267–18269.

Verkman, A. S., A. N. van Hoek, T. Ma, A. Frigeri, W. R. Skach, A. Mitra, B. K. Tamarappoo, and J. Farinas. 1996. Water transport across mammalian cell membranes. *Am. J. Physiol.* 270:C12–C30.

Wang, P., Z. F. Ba, J. Burkhardt, and I. H. Chaudry. 1993. Trauma-hemorrhage and resuscitation in the mouse: effects on cardiac output and organ blood flow. *Am. J. Physiol.* 264:H1166–H1173.

Wangensteen, O. D. 1974. Nonselective solute transport across the pulmonary epithelium. *In* Fluid and Solute Transport in the Airspaces of the Lungs, Vol. 79. R. M. Effros and H. K. Chang, editors. Marcel Dekker, New York. 1–56.